Elastic and anharmonic properties of pyridinium tetrafluoroborate ($[C_5NH_6]^+[BF_4]^-$≡$PyBF_4$): light scattering study of the phase transitions at various pressures

2001 J. Phys.: Condens. Matter 13 6563

(http://iopscience.iop.org/0953-8984/13/30/312)

INSTITUTE OF PHYSICS PUBLISHING JOURNAL OF PHYSICS: CONDENSED MATTER

J. Phys.: Condens. Matter **13** (2001) 6563–6576 PII: S0953-8984(01)22656-3

Elastic and anharmonic properties of pyridinium tetrafluoroborate ($[C_5NH_6]^+[BF_4]^- \equiv PyBF_4$): light scattering study of the phase transitions at various pressures

C Ecolivet[1], P Czarnecki[2], J Wasicki[2], S Beaufils[1], A Girard[1] and L Bobrowicz-Sarga[2]

[1] Groupe Matière Condensée et Materiaux—UMR CNRS 6626, Université de Rennes 1, Campus de Beaulieu, 35042 Rennes Cédex, France
[2] Institute of Physics, Adam Mickiewicz University, ul. Umultowska 85, PL-61-614 Poznan, Poland

Received 8 March 2001, in final form 30 May 2001
Published 13 July 2001
Online at stacks.iop.org/JPhysCM/13/6563

Abstract

The vibrational properties of pyridinium tetrafluoroborate crystals were studied by means of Brillouin scattering at atmospheric pressure, Raman scattering and neutron diffraction under high pressure.

It is shown that the elastic properties strongly reflect the molecular anisotropy of the pyridinium ions. The compressibility obtained from the Brillouin scattering study is in reasonable agreement with the results from neutron crystallography under pressure. Brillouin spectra reveal a small quasi-elastic component at room temperature, which is described by a coupled-susceptibilities formalism applied to the longitudinal mode and a relaxation mode. The mode Grüneisen parameters for all three phases that are found are determined from the pressure and temperature dependence of the Raman spectra and from neutron experiments.

(Some figures in this article are in colour only in the electronic version)

1. Introduction

Pyridinium tetrafluoroborate, $[C_5NH_6]^+[BF_4]^-$ (hereafter $PyBF_4$), is an ionic crystal but its physical properties are similar to those of molecular crystals, which means that van der Waals interactions play an important role. $PyBF_4$ crystallizes at room temperature in the centrosymmetric $R\bar{3}m$ space group [1, 2] with one pair of ions per cell as seen in figure 1. The flat pyridinium cation is perpendicular to the threefold axis—called here the c- or Z-axis—and located between two crystallographically equivalent anions. The D_{3d} site symmetry of the ions is a supergroup of the pyridinium cation symmetry group C_{2v}—then a rotational disorder

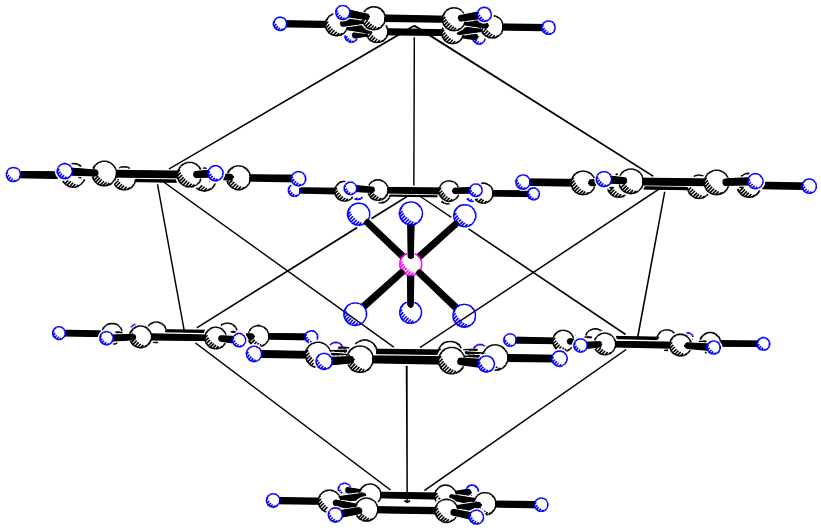

Figure 1. A view of the trigonal cell in a projection in a plane containing the threefold axis $\boldsymbol{c}$ which corresponds to the vertical diagonal. Pyridiniums ions are in the corners of the cell represented and define layers inside which the orientationally disordered BF_4 are lying. This ion, in the middle of the cell, is represented as a six-arm system in order to mimic the disorder.

around the threefold axis occurs—whereas the symmetry group T_d of BF_4 is neither a subgroup nor a supergroup of the site group, resulting in complete orientational disorder of the anion. Earlier NMR studies proved that reorientations of these pyridinium cations, as well as the anions in many pyridinium salts, occur [3–8]. In the structure, the planes of disordered cations are parallel to each other and perpendicular to the threefold axis of the trigonal system. The parallel orientation of the flat cation implies a strong anisotropy of the physical properties measured along and perpendicular to the pyridinium cation ring. $PyBF_4$ undergoes a sequence of structural phase transitions: $R\bar{3}m$ (I)–C2 (II)–P2 (III), and the transition at $T_1 = 238.7$ K between phases I and II is a ferroelectric one. The ferroelectric properties are in directions perpendicular to the threefold axis of the prototype phases, so $PyBF_4$ belongs to the group of multiaxial ferroelectrics and presents a continuous phase transition, which is exceptional for multiaxial ferroelectrics [1]. Although the complete structure has not been solved for the low-temperature phase, the symmetry of the intermediate phase (C2, $Z = 2$) implies parallel orientation of the flat cation and so strong anisotropy of the physical properties as in the high-temperature phase.

This paper reports vibrational spectroscopic studies by means of Brillouin and Raman scattering. Sound velocity measurements made by means of Brillouin scattering are related to the compound structure. The presence of a quasielastic component probably related to the disordered high-temperature structure could provide a means for estimating a correlation time. The Raman spectra measured at ambient and high pressure allowed us to calculate the Grüneisen parameters for the lattice and the internal modes. In order to estimate the Grüneisen parameter from the pressure shift of the Raman modes we have to use compressibility data obtained from neutron diffraction experiments where the lattice constants were determined under pressure. We compare and discuss the compressibility computed from the elastic constants and the pressure dependence of the lattice constants in the high-temperature phase. The Grüneisen parameters are obtained from temperature and pressure variations.

2. Brillouin scattering

Light scattering spectra were recorded either at 514.5 nm by using a single-mode Ar-ion laser or at 647.1 nm using a single-mode Kr-ion laser and a tandem arrangement of Fabry–Perot interferometers (Sandercock mounting), where each interferometer is triply passed, giving an overall contrast larger than 10^{11}. The advantage of this tandem arrangement of interferometers over a single one is that it removes the periodicity of the interferogram allowing, in the same spectrum, the observation of broad and narrow components without any confusion due to overlapping orders. Interference filters were also used in order to remove high-frequency Raman lines which could appear somewhere in the spectra. Different free spectral ranges between 5 cm^{-1} (1 cm^{-1} = 30 GHz) and 0.7 cm^{-1} have been used in order to give a full description of the low-frequency spectra. The polarization of the incident light was rotated by a half-wave plate and filtered by a Glan prism whereas the scattered light was when necessary analysed by another polarizing Glan prism. Spectra, after detection by a low-noise photomultiplier (EMI 9863B), were recorded, stored and processed on a PC.

2.1. Room temperature study

We have estimated the refractive indices of this crystal using different scattering geometries by using the Brillouin shift general formula:

$$\nu_B = \pm 2V \frac{\sqrt{(n_i^2 + n_s^2 - 2n_i n_s \cos\theta)}}{\lambda} \tag{1}$$

where ν_B is the Brillouin shift, n_i and n_s the refractive indices for the incident and scattered beams, θ the scattering angle, λ the laser wavelength and V the sound velocity. In particular, the so-called 'platelet' geometry [9] where the angle between the incident and scattered beams is 90° outside of the sample with an incident beam at 45° allows a direct measurement of the sound velocity in the platelet plane. In that case, the relation of the actual scattering angle inside the crystal to the refractive index is the reciprocal of the dependence in the Brillouin shift formula stated above, and the radical in formula (1) is replaced by $\sqrt{2}$. Taking this in conjunction with backscattering experiments probing the same phonon propagation direction, it is possible to extract an estimate of the refractive indices. The result is a positive uniaxial crystal with

$$n_o = 1.30 \pm 0.05 \qquad n_e = 1.48 \pm 0.05.$$

This large birefringence with such a small refractive index reflects the difference between the polarizabilities in and out of the plane of the pyridinium cation, whereas the contribution of the tetrafluoroborate anion is very small, as is usual with fluorine atoms, which have a small optical polarizability.

The angular dispersion of the sound velocities was determined by rotating the crystal around the principal directions and applying the Snell–Descartes law for the different light polarizations. More than 40 sound velocities were measured and assigned to the different acoustic polarizations. The best fit of the elastic constants which minimizes the relative uncertainties gives for the $\bar{3}m$ group with a specific mass of 1.56 g cm^{-3}

$$C_{11} = C_{22} = 21.5 \text{ GPa} \qquad C_{12} = 10.5 \text{ GPa}$$
$$C_{33} = 9.05 \text{ GPa} \qquad C_{13} = C_{23} = 8.0 \text{ GPa}$$
$$C_{44} = C_{55} = 2.2 \text{ GPa} \qquad C_{66} = (C_{11} - C_{12})/2 = 5.5 \text{ GPa}$$
$$C_{14} = -C_{24} = C_{56} = 1.75 \text{ GPa}.$$

The determination accuracy is a few per cent for diagonal constants and more probably about 10% for off-diagonal components, independently of the errors in the refractive indices, which are systematic ones. The elastic constants also reflect the anisotropy of the pyridinium ring since the longitudinal sound velocity in this plane (perpendicular to the threefold axis) is about $\sqrt{2}$ times the value along this axis, as can be seen in figures 2(a) and 2(b), which display the sound velocity polar diagrams in the principal crystallographic planes. The lines correspond to the velocity values computed from the Christoffel equations with the set of elastic constants.

A small quasielastic scattering component is also detected in all of the spectra recorded with a free spectral range of 5 cm^{-1} (150 GHz). At this scale, the high-frequency wing above 15 GHz is correctly fitted by any Lorentzian profile. However, such fits do not work for spectra recorded with a smaller spectral range, since the shape of the longitudinal Brillouin line does not correspond to a damped oscillator profile. It turns out that spectra are well described using coupled susceptibilities of the longitudinal acoustic mode with a relaxation mode characterized by a width of 5 GHz at 300 K. If the origin of this component can be related to a simple reorientation of an anisotropic group or ion, the corresponding relaxation time (30 ps) could be compatible with the reorientation of a deformed BF_4 anion, since a contribution from the anisotropic cation is precluded by the fact that this quasielastic component is observable for all directions and polarizations. However, this origin would require that the BF_4 tetrahedra be deformed, which is not obvious from the Raman studies.

The computed spectra were obtained through the convolution of an idealized computed apparatus function—taking into account the finesse of the reflectivity of the tandem arrangement—with the imaginary parts of the different components derived from the coupled-susceptibilities equations:

$$I(\omega)/(n(\omega)+1) = I_o\chi''_{oo}(\omega) + I_a\chi''_{aa}(\omega) + 2\sqrt{I_oI_a}\,\chi''_{ao}(\omega) \tag{2}$$

where the coupled susceptibilities are given by [11]

$$\begin{aligned}\chi_{ii}^{-1}(\omega) &= [1-\Delta^2\chi_j^o(\omega)\chi_i^o(\omega)]/\chi_i^o(\omega)\\ \chi_{ij}^{-1}(\omega) &= [1-\Delta^2\chi_j^o(\omega)\chi_i^o(\omega)]/\Delta\chi_j^o(\omega)\chi_i^o(\omega)\end{aligned} \tag{3}$$

where $i, j = a, o$ indicate the acoustic and relaxational origins whereas Δ is the coupling strength and the uncoupled susceptibilities are

$$\begin{aligned}\chi_o^{0-1} &= \Omega_o^2(1-\mathrm{i}\omega/\Gamma_o)\\ \chi_a^{0-1} &= \omega_a^2-\omega^2-\mathrm{i}\omega\gamma\end{aligned} \tag{4}$$

where Γ_o and γ are the linewidths (HWHM and FWHM respectively) of the relaxational and acoustic components, ω_a is the acoustic mode frequency and Ω_o is the bare (unknown) frequency of the overdamped optical mode generating the relaxational dynamics. Figure 3 shows a spectrum, recorded in a backscattering geometry along a direction at 15° from Z in the (YZ) plane, where experimental data are represented by dots. The Stokes side, on the right of the spectrum, has been fitted with usual oscillator profiles for all of the Brillouin lines (short dashes) and a Lorentzian shape (long dashes) for the quasielastic component; the solution shown after convolution with the apparatus function (continuous line) corresponds to the best description of the longitudinal Brillouin line and it implies consideration of a rather broad Lorentzian (20 GHz). Obviously this description fits neither between the Brillouin lines nor below; a better agreement there would imply a narrower quasielastic component which would fail in describing the spectrum at high frequencies. The anti-Stokes side, on the left of the spectrum, shows the result for the unconvoluted coupled susceptibilities of the longitudinal

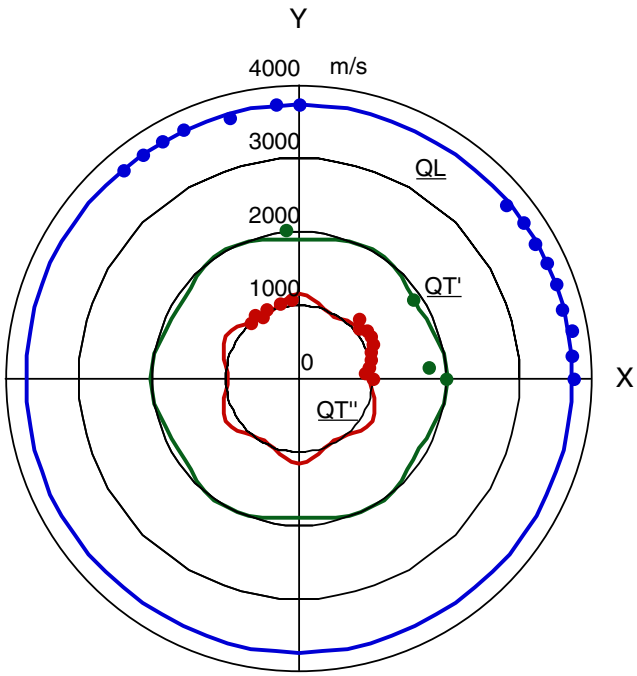

(a)

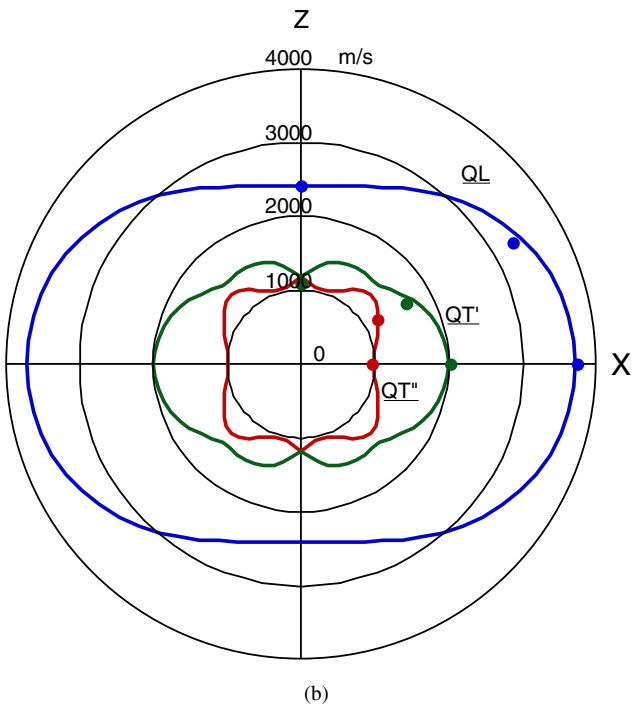

(b)

Figure 2. Polar sound velocity diagrams in the plane (XY) (a) and in the plane (XZ) (b). L, QL, T and QT refer to the polarization of the acoustic waves propagating along a general direction in the diagrams, Q indicating a mixed polarization of longitudinal and transverse character. Z stands for the threefold axis and X lies in the mirror plane.

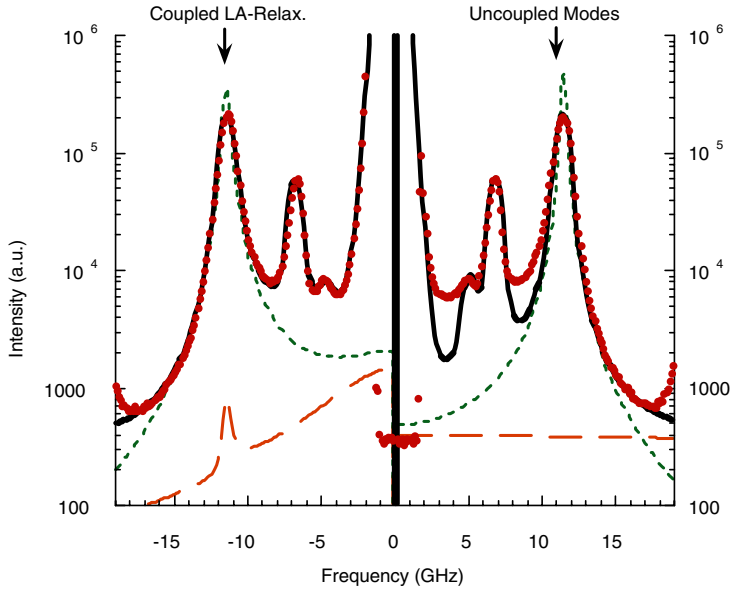

Figure 3. Brillouin and quasielastic spectra recorded for backscattering close to the Z-direction at room temperature. Dots show the experimental data. The Stokes (right) side shows the fit which gives the better description of the high-frequency side of the longitudinal Brillouin line as a continuous line, whereas the unconvoluted longitudinal Brillouin line and the quasielastic component are represented by short and long dashes. The anti-Stokes (left) side displays the best fit with a coupled-susceptibilities scheme: the lines with short and long dashes give the coupled acoustic and quasielastic contributions. The interference term cannot be displayed on a semilog plot.

mode (short dashes) and the relaxational mode (long dashes) with a reduced coupling strength $|\Delta/\Omega_o| = 3.2$ GHz; the interference term cannot be shown on a log scale since it changes sign at the acoustic frequency. Moreover, since the relaxational component is rather weak, this term, proportional to the square root of the product of the two intensities, is usually negligible; nevertheless it is included in the total convoluted intensity (continuous line). The resulting fit is obviously much better than the one on the Stokes side and the individual contributions reveal the mixing which occurs for the two components, each one presenting an anomaly at the pole of the susceptibility of the other one.

For a phonon wavevector along the X-direction, spectra recorded with an electric field polarized along Z or perpendicular to it have been fitted with the same coupling strength corrected on the basis of the ratio of the refractive indices but with different signs. We have found only one acceptable value of the quasielastic linewidth (5 GHz) which fits all of the spectra recorded with different free spectral ranges; it should be noticed that the longitudinal Brillouin shift is larger than this value and consequently the acoustic mode is not relaxed much by the quasielastic component. The longitudinal linewidth found in this fit is rather high: about 1 GHz, but this width is probably somewhat overestimated since the convoluted apparatus function is a calculated one which is only an approximation of the actual one.

2.2. Compressibility determination

We can compare the compressibility results obtained at room temperature by the two methods: the Brillouin scattering method that gives the tensor of the elastic constants and the method

based on the compressibility obtained from the pressure lattice constant measurements [10]. The inverse of the elastic constant tensor gives the compliance constant tensor:

$$(C_{ijkl})^{-1} = (S_{ijkl}).$$

After transformation we get

$s_{11} = s_{22} = 0.0887\ \text{GPa}^{-1}$ $s_{12} = -0.0327\ \text{GPa}^{-1}$
$s_{33} = 0.198\ \text{GPa}^{-1}$ $s_{13} = s_{23} = -0.0495\ \text{GPa}^{-1}$
$s_{44} = s_{55} = 0.59\ \text{GPa}^{-1}$ $s_{66} = 2(s_{11} - s_{12}) = 0.239\ \text{GPa}^{-1}$
$s_{14} = -s_{24} = s_{56}/2 = -0.0968\ \text{GPa}^{-1}$.

The volume compressibility in phase I is calculated from the equation

$$\beta = (2s_{11} + s_{33}) + 2(2s_{13} + s_{12}) = 0.112\ \text{GPa}^{-1}.$$

The volume compressibility obtained from the lattice constant determination under pressure is $0.126\ \text{GPa}^{-1}$. The agreement between the two methods is in the 10% range and looks satisfactory. However, if one considers the linear compressibility which is expressed as the relative change of dimension under pressure along a definite crystal direction, one can see that the linear compressibility is larger along the threefold axis perpendicular to the cation than in the perpendicular plane, but this anisotropy measured via the structure determination is somewhat larger than the one obtained from elastic measurements. One can also note that Brillouin scattering probes the adiabatic elastic constants, while in the high-pressure measurements the isothermal compressibility is obtained; however, the difference between the adiabatic and the isothermal compressibilities is expected to be small far from transition temperatures.

2.3. Temperature evolution

The change of Bravais lattice at the first phase transition between phases II and I implies that the related transition should display some ferroelastic features. Although the symmetry of the different phases precludes the occurrence of an acoustic soft mode, one may expect the observation of ferroelastic domains below T_1 since six orientational states and three ferroelastic domains are counted. The temperature evolution of the Brillouin spectra has been recorded for phonons propagating close to the threefold axis and another direction perpendicular to this axis (10° from the Y-direction in the (YZ) plane). Strikingly, there is no evidence of any expected splitting of any Brillouin line in the monoclinic phases. Along both directions the only anomalies in the frequency evolution are changes of slopes at both transition temperatures with a maximum slope in phase II (figures 4 and 5). This kind of evolution can be related to a biquadratic coupling of the order parameter with the elastic strains; if we admit that the relaxation time of the order parameter is too slow to give any relaxation at the Brillouin frequencies, we should also conclude that the changes of the elastic properties of the different domains remain very small at low temperatures. The evolution of the linewidths deconvoluted from an ideal apparatus function also show some minor anomalies in the overall decrease towards lower temperatures down to T_2 (figures 6 and 7). At lower temperatures, some lines display a slight increase or a plateau, which could suggest an unresolved splitting.

The quasielastic component is too weak to be followed reliably at low temperatures, but there is no sign of direct implications of this component in the critical dynamics at any transition. This suggests that it is not directly generated by the motion of ions and that it could come from higher-order interactions like fluctuations in the phonon density of states.

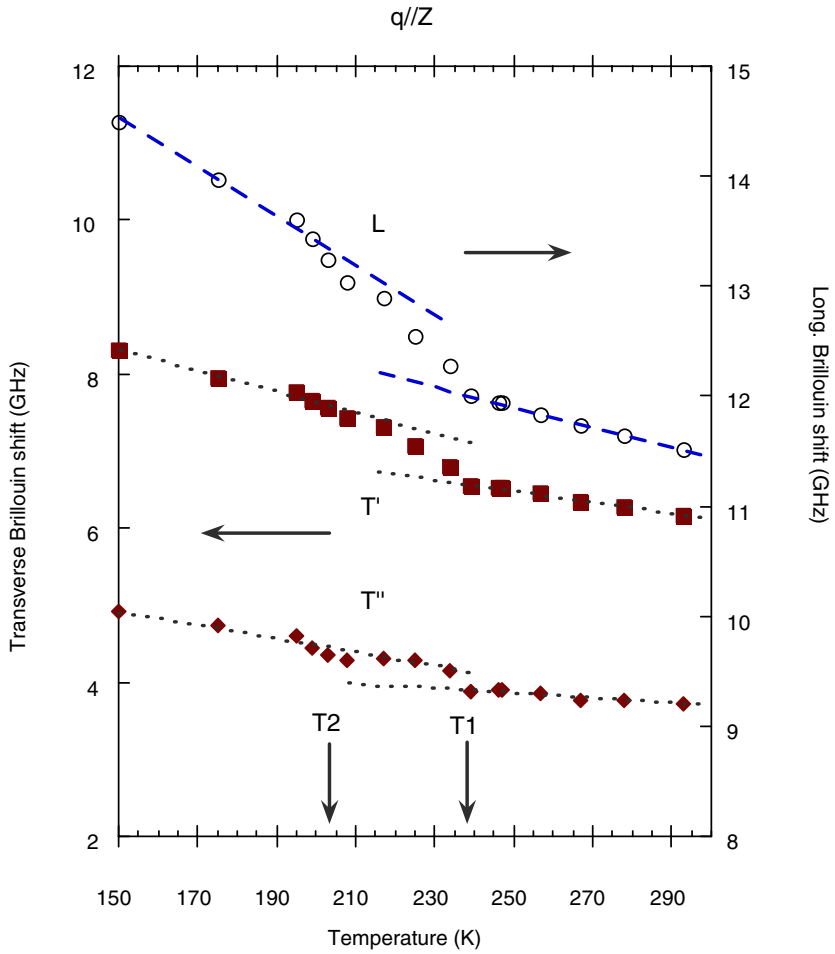

Figure 4. The temperature dependence of the Brillouin shifts of the longitudinal and transverse acoustic modes observed along a direction close to the Z-axis. Lines are guides for the eyes.

3. Raman scattering study of the anharmonic properties of the lattice and internal modes

3.1. Pressure dependence

The Raman high-pressure spectra were recorded with a Z 24 Dilor spectrometer. The hydrostatic high pressure was produced with a helium gas compressor. The lattice modes and some anion internal modes were recorded at atmospheric pressure and at 500 MPa at the temperatures of 85 K, 210 K and 296 K. The temperature and pressure dependences of the lattice constants were calculated from a high-pressure neutron diffraction investigation [10].

The mode Grüneisen parameter γ_i is defined by the equation $\gamma_i = -(\mathrm{d}\ln\nu_i/\mathrm{d}\ln V)$, or, in a more useful form,

$$\gamma_i = (1/\beta)(\mathrm{d}\ln\nu_i/\mathrm{d}p) = -(1/\alpha)(\mathrm{d}\ln\nu_i/\mathrm{d}T) \tag{5}$$

where ν_i is the frequency of the Raman mode, p is the pressure, β is the compressibility and α is the volume expansivity.

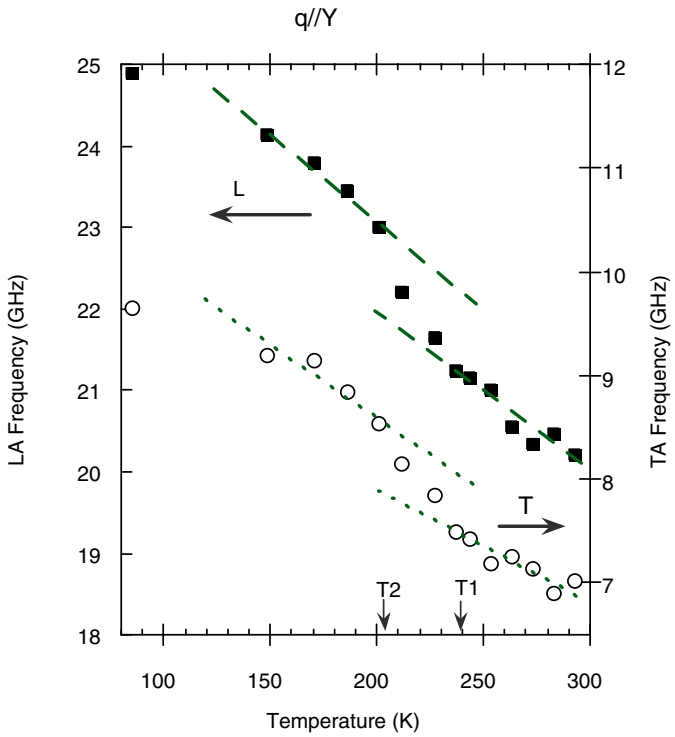

Figure 5. The temperature dependence of the Brillouin shifts of the longitudinal and transverse acoustic modes observed along a direction close to the Y-axis. Lines are guides for the eyes.

Grüneisen parameters describe the anharmonicity of the vibrations in a crystal. The vibration frequencies would be independent of both temperature and volume if the motions were completely harmonic. High values of the Grüneisen parameter represent a high anharmonicity of the vibrations in the crystal.

The lattice mode frequency range of the Raman spectrum presents, at room temperature, a broad component identical for all polarizations with a non-negligible amount of quasielastic scattering probably related to the disorder. From the point of view of the statistical symmetry created by dynamical disorder, a doubly degenerate E_g mode is expected.

It should consist in anti-rotations perpendicular to the c-direction. Its large intensity is in agreement with anisotropic motions of the cations out of their plane. The temperature evolution of these spectra shows strong evidence of increasing order in the low-temperature phases through a decreasing damping. The fit of the spectra cannot be reliably made above 120 K, so we only consider the evolution of this line.

The evolution of the high-pressure dependence of this mode is presented in figure 8 for all the three phases. The frequency of this mode increases normally with pressure. The Grüneisen parameter calculated for this lattice frequency from equation (5) is presented in table 1 for phases I and III. The main source of error lies in the compressibility, with a relative accuracy in the 10% range, resulting in relative errors of about 15% in the Grüneisen parameter. Accordingly it is difficult to see any differences between phases I and III with $\gamma = 2.1$.

One can see (table 1) that the shifts of the lattice mode frequencies under high pressure are similar for the two phases. For the high-temperature disordered phase I, there is only one broad peak. According to the symmetry changes [2], all modes could become Raman active

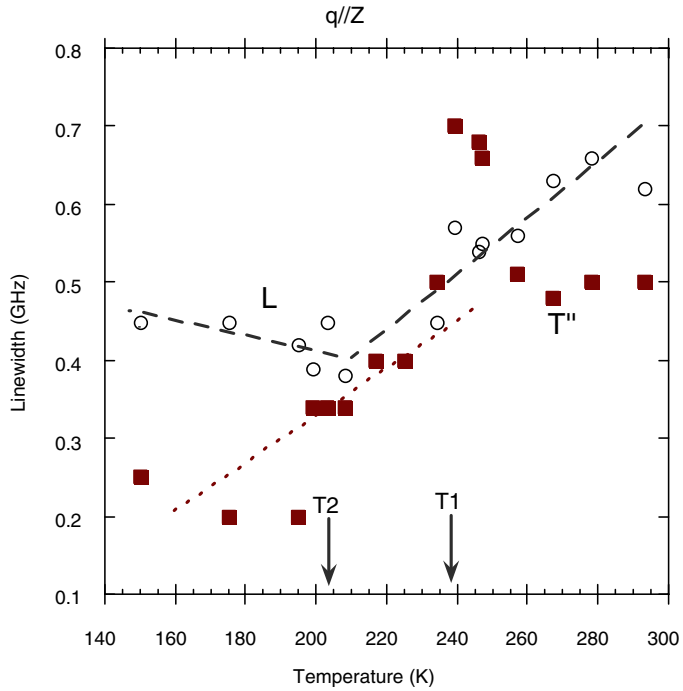

Figure 6. The temperature dependence of the Brillouin linewidths of the longitudinal and transverse acoustic modes observed along a direction close to the Z-axis. Lines are guides for the eyes.

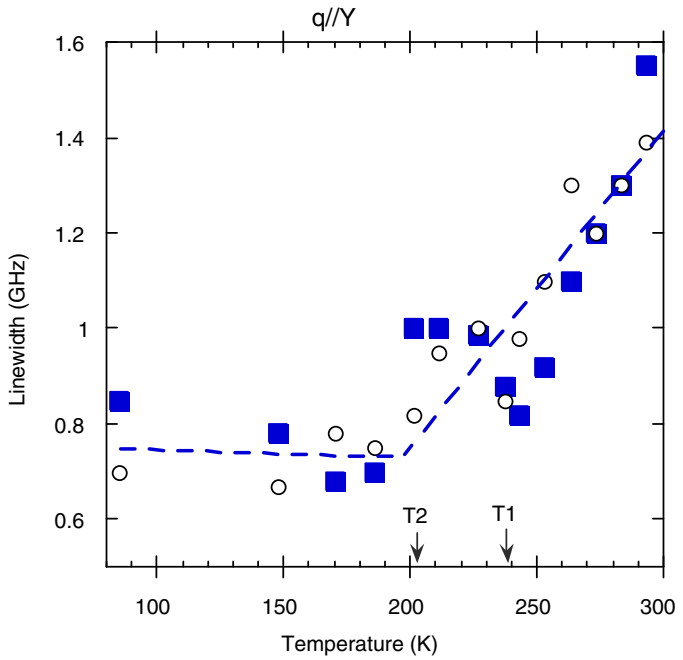

Figure 7. The temperature dependence of the Brillouin linewidths of the longitudinal (○) and transverse (■) acoustic modes observed along a direction close to the Y-axis. Lines are guides for the eyes.

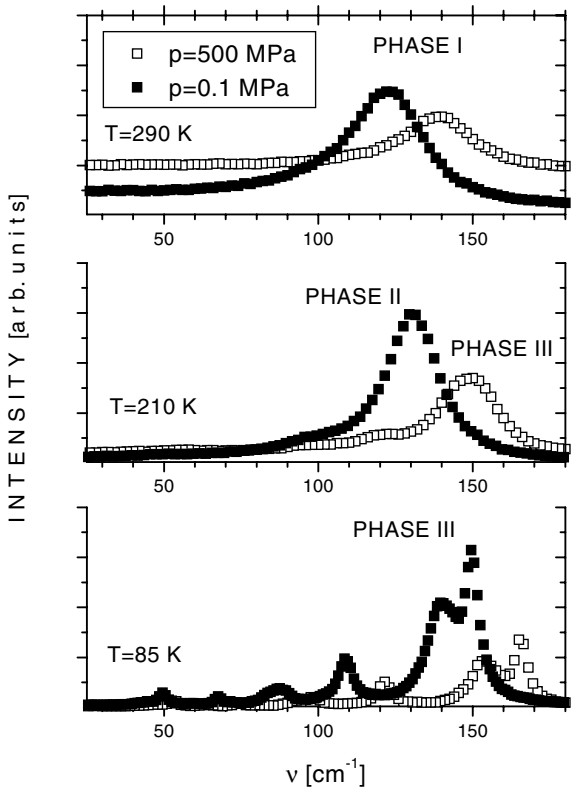

Figure 8. Low-frequency Raman spectra for the three different phases of the crystal at atmospheric pressure and 500 MPa (5 kbar).

Table 1. The main lattice mode parameters for phases I and III.

Lattice modes	$T = 296$ K	$T = 85$ K
ν_i (cm^{-1})	123	149
Linewidth (cm^{-1})	16	16
$d \ln \nu_i / dp$ (GPa^{-1})	0.260	0.214
Compressibility, β (GPa^{-1})	0.126	0.101
Grüneisen parameter, $\gamma_i = (1/\beta)(d \ln \nu_i / dp)$	2.1	2.1

in phase II but they remain broad and unresolved due to the remaining disorder, while more peaks are observed in the ordered phase III.

The pressure sensitivity is stronger for the E_g lattice mode (table 1) than for the internal anion mode (table 2) which appears also as a rather weak and broad component for phase I, which then splits into two broad components for phase II which also seem to split in phase III. This lower sensitivity is expected since the rather weak ionic and van der Waals interactions are much smaller than the intramolecular forces. It results in a low value of the Grüneisen parameter of 0.2 for the intramolecular vibration modes, an order of magnitude less than that of the lattice mode. In order to find any difference between the behaviours of the different phases we tried to obtain another determination of the Grüneisen parameters through the thermal dependence of the Raman frequencies.

Table 2. The anion mode parameters for phases I and III.

BF_4-anion modes	$T = 296$ K	$T = 85$ K
ν_i (cm^{-1})	352	352
Linewidth (cm^{-1})	4	3
$d \ln \nu_i / dp$ (GPa^{-1})	0.023	0.017
Compressibility, β (GPa^{-1})	0.126	0.101
Grüneisen parameter, $\gamma_i = (1/\beta)(d \ln \nu_i / dp)$	0.18	0.17

3.2. Temperature dependence

Determination of the Grüneisen parameters from temperature studies requires knowledge of the volume variation versus temperature. This result is available from the measurements of the lattice constants by neutron crystallography for a few temperatures and pressures [10]. In order to compare the results for all three phases we transformed the lattice constants of the monoclinic II and III phases to a pseudo-hexagonal system, in which the highest anisotropy is between the directions $\boldsymbol{c}$ and $\boldsymbol{a}$. The results for the temperature dependence are presented in figure 9. One can see that the temperature slope of the lattice constant c is significantly higher than those of the lattice constants a and b. This anisotropy is quite similar to that of the linear compressibility and persists in phase III, which suggests that the structure of this phase is also planar. In particular, one cannot expect it to be generated by a strong tilt of the cations out of their layer.

The temperature dependence of the main Raman lattice mode is presented in figure 9. Knowing the volume and the Raman lattice mode dependence versus temperature (figure 9) we can estimate the Grüneisen parameter for the external mode from equation (5). In that case, $\gamma_i = 1.8$, 2.7 and 1.5 for phases I, II and III, respectively. The difference between the Grüneisen parameters obtained from high-pressure experiments (table 1) and from temperature variations is at the limit of the experimental errors but, if we compare to the expansion measurements from reference [12], the different values of γ_i agree well with the expansivity of the three phases. In particular, the intermediate phase II reveals the largest expansivity.

4. Conclusions

This paper reports a study of the elastic properties of pyridinium tetrafluoroborate crystals in their high-temperature trigonal phase based on determination of all of the elastic constants from Brillouin scattering measurements. It is clearly shown that these properties as well as the refractive indices are strongly affected by the molecular anisotropy of the pyridinium ions. The compressibility data obtained by this technique are in reasonable agreement with the results from neutron crystallography under pressure. Brillouin spectra clearly reveal a small quasielastic component at room temperature, which is in fact coupled to longitudinal acoustic modes along all directions. The coupled-susceptibilities formalism allows a good fit of all of the spectra by changing in some cases the sign of the coupling constant for different polarizations. The linewidth of this quasielastic component is too small to produce a noticeable relaxation of the acoustic modes; hence acoustic anomalies recorded at the phase transitions do not reveal a relaxational behaviour. Since it is very likely that the pyridinium tetrafluoroborate crystal undergoes order–disorder transitions with a progressive orientational ordering, one could expect to observe some narrowing of the quasielastic component on decreasing the temperature. However, this signal is already weak at room temperature and becomes rapidly very weak, which precludes the observation of its evolution.

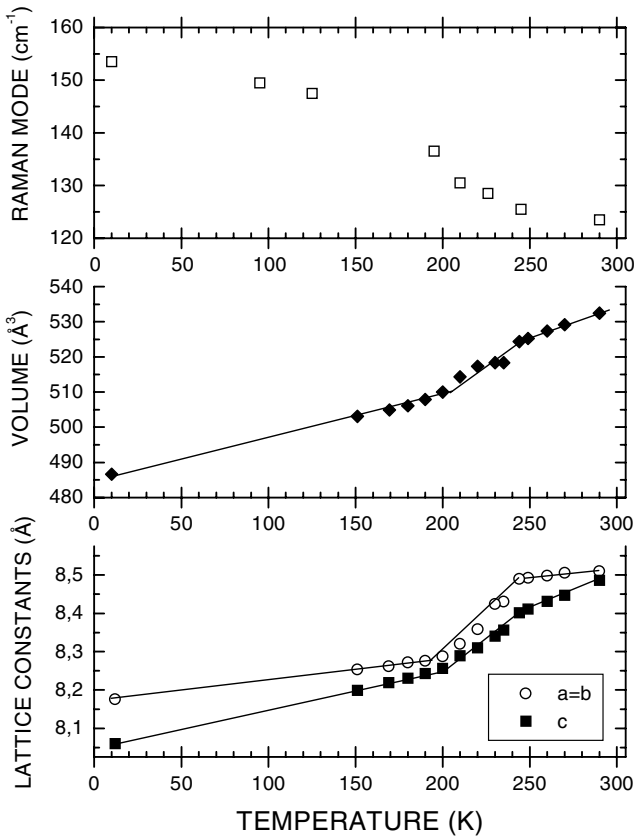

Figure 9. The Raman frequency of the E_g lattice mode and volume and lattice constants versus temperature at atmospheric pressure.

A striking feature of the low-temperature Brillouin spectra is the absence of any splitting of the acoustic frequencies, but the elastic anisotropy of the longitudinal acoustic mode in the (XY) plane is so small that any disorientation of the domains will not cause the appearance of a different Brillouin shift close to the transition temperature and we may only expect a splitting at lower temperatures, where the order parameter will be significantly different from zero. The slight increase of the Brillouin linewidth below the second transition temperature could be evidence of this tendency.

The determination of the Grüneisen parameter, which used reliable compressibility data, is rather new for this class of molecular–ionic compounds. The Grüneisen parameters clearly show a much stronger pressure effect on the external modes than on the internal modes like in usual van der Waals molecular crystals.

Acknowledgments

This work was partly supported by the State Committee for Scientific Research under Grant No 2P03B15615. The authors wish to thank particularly J C Ameline and S Lewicki for their help during the pressure experiments.

References

[1] Czarnecki P, Katrusiak A, Szafraniak I and Wasicki J 1998 *Phys. Rev.* B **57** 3326
[2] Czarnecki P, Wasicki J, Katrusiak A, Ecolivet C, Girard A and Belushkin A 1997 *Physica* B **102–103** 234
[3] Czarnecki P, Nawrocik W, Pajak Z and Wasicki J 1994 *J. Phys. C: Solid State Phys.* **6** 4955
[4] Czarnecki P, Wasicki J, Pajak Z, Goc R, Maluszynska H and Habrylo S 1997 *J. Mol. Struct.* **404** 175
[5] Wasicki J, Pajak Z and Kozak A 1990 *Z. Naturf.* a **45** 33
[6] Wasicki J, Nawrocik W, Pajak Z, Natkaniec I and Belushkin A V 1989 *Phys. Status Solidi* a **114** 497
[7] Ripmeester J 1976 *Can. J. Chem.* **54** 3453
[8] Copeland R F, Conner S H and Meyers E A 1966 *J. Phys. Chem.* **70** 1288
[9] Vaughan J M 1976 *Phys. Lett.* A **58** 325
[10] Bobrowicz-Sarga L, Czarnecki P, Lewicki S, Natkaniec I and Wasicki J 2000 *Mater. Sci. Forum* **321–324** 1107
[11] Katiyar R S, Ryan J F and Scott J F 1971 *Phys. Rev.* B **4** 2635
[12] Szafraniak I, Czarnecki P and Mayr P U 2000 *J. Phys.: Condens. Matter* **12** 643